PHYSOR 2004 -The Physics of Fuel Cycles and Advanced Nuclear Systems: Global Developments
Chicago, Illinois, April 25-29, 2004, on CD-ROM, American Nuclear Society, Lagrange Park, IL. (2004)

A First-Order Spherical Harmonics Formulation Compatible with the Variational Nodal Method

M. A. Smith[1], E. E. Lewis[2], G. Palmiotti[1] and W. S. Yang[1]
[1]*Argonne National Laboratory, 9700 South Cass Avenue, Argonne, Illinois 60439*
[2]*Northwestern University, Department of Mechanical Engineering, Evanston, Illinois 60208*

A spherical harmonics method based upon the first-order transport equation is formulated and implemented into VARIANT [1,2], a variational nodal transport code developed at Argonne National Laboratory. The spatial domain is split into hybrid finite elements, called nodes, where orthogonal polynomial spatial trial functions are used within each node and spatial Lagrange multipliers are used along the node boundaries. The internal angular approximation utilizes a complete odd-order set of spherical harmonics. Along the nodal boundaries, even and odd-order Rumyantsev interface conditions are combined with the spatial Lagrange multipliers to couple the nodes together. The new method is implemented in Cartesian x-y geometry and used to solve a fixed source benchmark problem.

KEYWORDS: neutron transport, nodal method, spherical harmonics, first-order form, VARIANT, void node problems

1. Introduction

The variational nodal method implemented in VARIANT [1,2] cannot be applied directly to voided nodes because of the cross section appearing in the denominator of the second-order even-parity equation. Problems are also encountered when very low-density media occupy a node. A potential alternative for these situations is to form the nodal response matrix using the first-order form of the transport equation, for then the cross section no longer appears in the denominator.

In this work a weighted residual approach is applied to the first-order form of the transport equation assuming the presence of isotropic scattering as well as an isotropic source. To maintain consistency, the same spatial trial functions used in VARIANT are applied both within the node and along the interfaces. Similarly, spherical harmonic approximations are applied to the angular variables. The result is an approximation for the angular flux within the node in terms of the group source and the neutron flux incident on the nodal surface. Given the nodal angular flux solution, the boundary angular flux distribution can be expressed in terms of the interface variables used in VARIANT. This is necessary if first- and second-order methods are to be used in conjunction with one another, which is the underlying goal of this work.

The response matrix formulation was implemented in MATHCAD [3] to examine the properties of the response matrix and apply them to model problems of limited problem size. The resulting response matrices were then imported into the VARIANT code where larger problems can be solved. The solutions obtained using the new method are promising and the method appears to be able to treat problems that have void regions.

2. Theory

The starting point for the new method is the first-order form of the transport equation with total and isotropic scattering cross sections σ and σ_s given by Eq. (1).

$$\hat{\Omega}\cdot\vec{\nabla}\psi(\vec{r},\hat{\Omega})+\sigma_t\psi(\vec{r},\hat{\Omega})-\sigma_s\phi(\vec{r})-s(\vec{r})=0, \qquad \vec{r}\in V, \qquad (1)$$

Using nodal decomposition of the spatial domain, we obtain the general boundary condition for each node where $\hat{n}$ is the outward normal.

$$\psi(\vec{r},\hat{\Omega})-\psi_\lambda(\vec{r},\hat{\Omega})=0, \qquad \vec{r}\in\Gamma, \hat{n}\cdot\hat{\Omega}<0 \qquad (2)$$

These equations are multiplied by the weight vector $\mathbf{f}(\vec{r})$ and integrated over the nodal spatial domain to obtain the weighted residuals where bold faced lower and upper case symbols indicate column vectors and matrices, respectively.

$$\int dV\,\mathbf{f}\left[\hat{\Omega}\cdot\vec{\nabla}\psi+\sigma_t\psi-\sigma_s\phi-s\right]-\int_{\hat{\Omega}\cdot\hat{n}<0} d\Gamma\hat{\Omega}\cdot\hat{n}\mathbf{f}\left[\psi-\psi_\lambda\right]=0 \qquad (3)$$

Applying the divergence theorem to the streaming term and substituting the result into Eq. (3) yields

$$-\int dV\ \hat{\Omega}\cdot\vec{\nabla}\mathbf{f}\,\psi+\int dV\,\mathbf{f}\left[\sigma_t\psi-\sigma_s\phi-s\right]+\int_{\hat{\Omega}\cdot n>0} d\Gamma\,\hat{\Omega}\cdot\hat{n}\mathbf{f}\,\psi+\int_{\hat{\Omega}\cdot n<0} d\Gamma\,\hat{\Omega}\cdot\hat{n}\mathbf{f}\,\psi_\lambda=0. \qquad (4)$$

The general convex surface Γ is replaced by a sum of flat surfaces Γ_γ each with an outward normal $\hat{n}_\gamma$ such that each node is consistent with that defined in the VARIANT code [2].

2.1 Spatial Discretization

The spatial component of the angular flux is approximated within the node by

$$\psi(\vec{r},\hat{\Omega})=\mathbf{f}^T(\vec{r})\boldsymbol{\psi}(\hat{\Omega}), \qquad \vec{r}\in V \qquad (5)$$

$$\phi(\vec{r})=\mathbf{f}^T(\vec{r})\int d\Omega\,\boldsymbol{\psi}(\hat{\Omega})=\mathbf{f}^T(\vec{r})\boldsymbol{\psi}_o, \qquad \vec{r}\in V \qquad (6)$$

and the boundary condition by

$$\psi_\lambda(\vec{r},\hat{\Omega})=\mathbf{h}_\gamma^T(\vec{r})\boldsymbol{\psi}_{\lambda\gamma}(\hat{\Omega}), \qquad \vec{r}\in\Gamma_\gamma, \hat{n}_\gamma\cdot\hat{\Omega}<0 \qquad (7)$$

Inserting these approximations into Eq. (4) yields

$$\begin{aligned}&\left[-\hat{\Omega}\cdot\int dV(\vec{\nabla}\mathbf{f})\mathbf{f}^T+\int dV\sigma_t\mathbf{f}\mathbf{f}^T+\sum_{\hat{\Omega}\cdot\hat{n}_\gamma>0}\hat{\Omega}\cdot\hat{n}_\gamma\int_\gamma d\Gamma\,\mathbf{f}\mathbf{f}^T\right]\boldsymbol{\psi}(\hat{\Omega})\\&=\int dV\sigma_s\mathbf{f}\mathbf{f}^T\int d\Omega'\,\boldsymbol{\psi}(\hat{\Omega}')+\mathbf{s}-\sum_{\hat{\Omega}\cdot\hat{n}_\gamma<0}\hat{\Omega}\cdot\hat{n}_\gamma\int_\gamma d\Gamma\,\mathbf{f}\,\mathbf{h}_\gamma^T\boldsymbol{\psi}_{\lambda\gamma}(\hat{\Omega})\end{aligned}, \qquad (8)$$

and

$$\mathbf{s}=\int dV\,\mathbf{f}\,s. \qquad (9)$$

These equations can be compacted to obtain Eq. (10), by defining the integrals of the spatial trial functions as matrices and writing $\hat{\Omega}\cdot\int dV(\vec{\nabla}\mathbf{f})\mathbf{f}^T$ in terms of the direction cosines of $\hat{\Omega}$.

$$\left[-\sum_k\Omega_k\mathbf{U}_k+\mathbf{F}_t+\sum_{\hat{\Omega}\cdot\hat{n}_\gamma>0}\hat{\Omega}\cdot\hat{n}_\gamma\mathbf{W}_\gamma\right]\boldsymbol{\psi}(\hat{\Omega})=\mathbf{F}_s\int d\Omega'\,\boldsymbol{\psi}(\hat{\Omega}')+\mathbf{s}-\sum_{\hat{\Omega}\cdot\hat{n}_\gamma<0}\hat{\Omega}\cdot\hat{n}_\gamma\mathbf{D}_\gamma\boldsymbol{\psi}_{\lambda\gamma}(\hat{\Omega}) \qquad (10)$$

2.2 Spherical Harmonics Approximation

Next, $\mathbf{y}(\hat{\Omega})$, a vector of orthonormal spherical harmonics of order *N,* is used to approximate the angular component of the angular flux. The expansion takes the form

$$\boldsymbol{\psi}(\hat{\Omega}) = \mathbf{y}^T(\hat{\Omega}) \otimes \mathbf{I}_s \boldsymbol{\Psi}, \tag{11}$$

The identity matrices $\mathbf{I}_s$ and $\mathbf{I}_\Omega$ have the dimensions of **f** and **y**, respectively, and together they form the identity, $\mathbf{I} = \mathbf{I}_s \otimes \mathbf{I}_\Omega$. $\boldsymbol{\Psi}$ is a vector of unknown coefficients for the angular flux expansion which can be written as

$$\boldsymbol{\Psi} = \int d\Omega \left(\mathbf{y}(\hat{\Omega}) \otimes \mathbf{I}_s \right) \boldsymbol{\psi}(\hat{\Omega}). \tag{12}$$

Once $\boldsymbol{\Psi}$ has been determined, the angular flux may be constructed within the node by combining Eqs. (5) and (11) to obtain

$$\psi(\vec{r}, \hat{\Omega}) = \mathbf{y}^T(\hat{\Omega}) \otimes \mathbf{f}^T(\vec{r}) \boldsymbol{\Psi}. \tag{13}$$

Inserting Eq. (11) into Eq. (10), weighting it with the vector $\mathbf{y}(\hat{\Omega}) \otimes \mathbf{I}_s$, and integrating over angle we obtain Eq. (14).

$$\left[-\sum_k \int d\Omega\ \Omega_k \mathbf{y}\mathbf{y}^T \otimes \mathbf{U}_k + \mathbf{I}_\Omega \otimes \mathbf{F}_t + \sum_\gamma \int_{\hat{\Omega}\cdot\hat{n}_\gamma > 0} d\Omega\ \hat{\Omega}\cdot\hat{n}_\gamma \mathbf{y}\mathbf{y}^T \otimes \mathbf{W}_\gamma - \int d\Omega\, \mathbf{y} \int d\Omega'\, \mathbf{y}^T \otimes \mathbf{F}_s \right] \boldsymbol{\Psi} \tag{14}$$
$$= \int d\Omega\, \mathbf{y} \otimes \mathbf{s} - \sum_\gamma \int_{\hat{\Omega}\cdot\hat{n}_\gamma < 0} d\Omega\ \hat{\Omega}\cdot\hat{n}_\gamma \mathbf{y} \otimes \mathbf{D}_\gamma \boldsymbol{\psi}_{\lambda\gamma}$$

Eq. (14) can be rewritten in the matrix form

$$\mathbf{A}\boldsymbol{\Psi} = \mathbf{J} \otimes \mathbf{s} - \sum_\gamma \int_{\hat{\Omega}\cdot\hat{n}_\gamma < 0} d\Omega\ \hat{\Omega}\cdot\hat{n}_\gamma \mathbf{y}(\hat{\Omega}) \otimes \mathbf{D}_\gamma \boldsymbol{\psi}_{\lambda\gamma}(\hat{\Omega}). \tag{15}$$

Inverting **A** and solving for $\boldsymbol{\Psi}$ yields

$$\boldsymbol{\Psi} = \mathbf{q} - \sum_\gamma \mathbf{A}^{-1} \int_{\hat{\Omega}\cdot\hat{n}_\gamma < 0} d\Omega\ \hat{\Omega}\cdot\hat{n}_\gamma \mathbf{y}(\hat{\Omega}) \otimes \mathbf{D}_\gamma \boldsymbol{\psi}_{\lambda\gamma}(\hat{\Omega}). \tag{16}$$

The angular flux within the node can be reconstructed using Eq. (13).

2.3 Interface Conditions

Next, $\boldsymbol{\psi}_{\lambda\gamma}(\hat{\Omega})$, the vector of spatial moments of the angular flux on the node surface, must be related to the even- and odd-parity space-angle moments employed in VARIANT. In VARIANT, even- and odd-parity spherical harmonics expansions are used to represent the angular flux distribution within the node volume and on its surface, respectively. These expansions can be combined to express the space-angle distribution of the flux at the nodal surface as

$$\psi(\vec{r}, \hat{\Omega}) = \mathbf{y}_+^T(\hat{\Omega}) \otimes \mathbf{f}^T(\vec{r}) \boldsymbol{\xi} + \mathbf{y}_-^T(\hat{\Omega}) \mathbf{K}_\gamma \boldsymbol{\Lambda} \otimes \mathbf{h}^T(\vec{r}) \boldsymbol{\chi}_\gamma, \qquad \vec{r} \in \Gamma_\gamma. \tag{17}$$

Here, $\mathbf{f}(\vec{r})$ and $\mathbf{h}(\vec{r})$ are the same vectors of continuous trial functions defined for $\vec{r} \in V$ and $\vec{r} \in \Gamma$, respectively. $\mathbf{y}_+(\hat{\Omega})$ and $\mathbf{y}_-(\hat{\Omega})$ are vectors of the even- and odd-parity spherical harmonics.

In VARIANT, the odd-parity spherical harmonics are rotated to align the polar angle with the outgoing normal. This allows the boundary condition implementations to be the same on all

surfaces. The square matrix $\mathbf{K}_\gamma$ is defined to represent the rotation from $\hat{n}_\gamma$ to the reference direction $\hat{n}_o$ as shown in Eq. (19).

$$\mathbf{y}_-(\hat{\Omega}) = \mathbf{K}_\gamma \mathbf{y}_{\gamma-}(\hat{\Omega}) \tag{18}$$

$$\mathbf{K}_\gamma = \int d\Omega\, \mathbf{y}_-(\hat{\Omega})\mathbf{y}_{\gamma-}^T(\hat{\Omega}) \tag{19}$$

At this point we define the $\mathbf{\Lambda}$ matrix, which extracts the necessary linear combinations of the odd-parity flux moments that must be held continuous across the nodal interfaces. In VARIANT, two sets of angular interface functions, and thus two $\mathbf{\Lambda}$, have been defined: the LI (linearly independent) set [4] and the Rumyantsev set [5].

The hybrid nodal method, upon which VARIANT is based, requires both $\boldsymbol{\chi}_\gamma$ and $\boldsymbol{\varphi}_\gamma$ to be continuous across nodal interfaces, where $\boldsymbol{\varphi}_\gamma$ is given by Eqs. (20) and (21).

$$\boldsymbol{\varphi}_\gamma = \mathbf{\Lambda}^T \mathbf{K}_\gamma^T \mathbf{E}_\gamma^T \otimes \mathbf{D}_\gamma^T \boldsymbol{\xi} \tag{20}$$

$$\mathbf{E}_\gamma = \int d\Omega\, \hat{\Omega}\cdot\hat{n}_\gamma \mathbf{y}_+(\hat{\Omega})\mathbf{y}_-^T(\hat{\Omega}) \tag{21}$$

The boundary flux $\boldsymbol{\psi}_{\lambda\gamma}(\hat{\Omega})$ in Eq. (16) can be expressed in terms of $\boldsymbol{\varphi}_\gamma$ and $\boldsymbol{\chi}_\gamma$ as shown in Eq. (22).

$$\boldsymbol{\psi}_{\lambda\gamma}(\hat{\Omega}) = \mathbf{y}_+^T(\hat{\Omega})(\mathbf{\Lambda}^T\mathbf{K}_\gamma^T\mathbf{E}_\gamma^T)^{-1} \otimes \mathbf{I}_\gamma \boldsymbol{\varphi}_\gamma + \mathbf{y}_-^T(\hat{\Omega})\mathbf{K}_\gamma\mathbf{\Lambda} \otimes \mathbf{I}_\gamma \boldsymbol{\chi}_\gamma \qquad \hat{n}_\gamma\cdot\hat{\Omega} < 0 \tag{22}$$

Eq. (22) can be multiplied by $\mathbf{D}_\gamma$ and the properties of $\otimes$ used to obtain

$$\mathbf{D}_\gamma\boldsymbol{\psi}_{\lambda\gamma}(\hat{\Omega}) = \mathbf{y}_+^T(\hat{\Omega})(\mathbf{\Lambda}^T\mathbf{K}_\gamma^T\mathbf{E}_\gamma^T)^{-1} \otimes \mathbf{D}_\gamma\boldsymbol{\varphi}_\gamma + \mathbf{y}_-^T(\hat{\Omega})\mathbf{K}_\gamma\mathbf{\Lambda} \otimes \mathbf{D}_\gamma\boldsymbol{\chi}_\gamma\,. \tag{23}$$

Finally, Eq. (23) is substituted into Eq. (16) resulting in

$$\mathbf{\Psi} = \mathbf{q} - \sum_\gamma \left[\mathbf{M}_\gamma^+(\mathbf{\Lambda}^T\mathbf{K}_\gamma^T\mathbf{E}_\gamma^T)^{-1} \otimes \mathbf{D}_\gamma\boldsymbol{\varphi}_\gamma + \mathbf{M}_\gamma^-\mathbf{K}_\gamma\mathbf{\Lambda} \otimes \mathbf{D}_\gamma\boldsymbol{\chi}_\gamma \right], \tag{24}$$

where

$$\mathbf{M}_\gamma^\pm = \mathbf{A}^{-1} \int\limits_{\hat{\Omega}\cdot\hat{n}_\gamma<0} d\Omega\; \hat{\Omega}\cdot\hat{n}_\gamma \mathbf{y}(\hat{\Omega}) \otimes \mathbf{I}_s \mathbf{y}_\pm^T(\hat{\Omega})\,. \tag{25}$$

2.4 Response Matrix Form

To obtain response matrices, continuity conditions must be imposed on the angular flux across the interfaces. Recall that the boundary condition given by Eq. (22), which specifies the angular distribution of the incoming flux (for $\hat{n}_\gamma\cdot\hat{\Omega} < 0$) in terms of $\boldsymbol{\varphi}_\gamma$ and $\boldsymbol{\chi}_\gamma$, is the approximation to Eq. (2).

The even- and odd-parity components can be treated separately, thereby obtaining Eqs. (26) and (27) where the matrices of Eq. (28) have been used.

$$\boldsymbol{\varphi}_\gamma = \mathbf{\Lambda}^T\mathbf{K}_\gamma^T\mathbf{E}_\gamma^T\Xi_+ \otimes \mathbf{D}_\gamma^T\mathbf{\Psi} \tag{26}$$

$$\boldsymbol{\chi}_\gamma = \left(\mathbf{\Lambda}^T\mathbf{\Lambda}\right)^{-1}\mathbf{\Lambda}^T\mathbf{K}_\gamma^T\Xi_- \otimes \mathbf{D}_\gamma^T\mathbf{\Psi} \tag{27}$$

$$\Xi_\pm = \int d\Omega\; \mathbf{y}_\pm(\hat{\Omega})\mathbf{y}^T(\hat{\Omega}) \tag{28}$$

Continuity can be imposed on Eq. (26), Eq. (27), or a linear combination of the two. Using weights of ½ a and *b*, which are free parameters, Eqs. (26) and (27) can be linearly combined as shown in Eqs. (29) and (30).

$$\tfrac{1}{2} a\boldsymbol{\varphi}_\gamma + b\boldsymbol{\chi}_\gamma = \boldsymbol{\Pi}_\gamma \boldsymbol{\Psi} \tag{29}$$

$$\boldsymbol{\Pi}_\gamma = \left[\tfrac{1}{2} a\boldsymbol{\Lambda}^T \mathbf{K}_\gamma^T \mathbf{E}_\gamma^T \Xi_+ + b\left(\boldsymbol{\Lambda}^T \boldsymbol{\Lambda}\right)^{-1} \boldsymbol{\Lambda}^T \mathbf{K}_\gamma^T \Xi_- \right] \otimes \mathbf{D}_\gamma^T \tag{30}$$

Combining Eqs. (24) and (30), Eq. (31) is obtained.

$$\tfrac{1}{2} a\boldsymbol{\varphi}_\gamma + b\boldsymbol{\chi}_\gamma = \boldsymbol{\Pi}_\gamma \mathbf{q} - \sum_{\gamma'} \boldsymbol{\Pi}_\gamma \mathbf{M}_{\gamma'}^+ (\boldsymbol{\Lambda}^T \mathbf{K}_{\gamma'}^T \mathbf{E}_{\gamma'}^T)^{-1} \otimes \mathbf{D}_{\gamma'} \boldsymbol{\varphi}_{\gamma'} - \sum_{\gamma'} \boldsymbol{\Pi}_\gamma \mathbf{M}_{\gamma'}^- \mathbf{K}_{\gamma'} \boldsymbol{\Lambda} \otimes \mathbf{D}_{\gamma'} \boldsymbol{\chi}_{\gamma'} \tag{31}$$

The variable transformation implemented in VARIANT, shown here as Eq. (32), can now be implemented in Eq. (31) to yield

$$\mathbf{j}^\pm = \tfrac{1}{4} \boldsymbol{\varphi} \pm \tfrac{1}{2} \boldsymbol{\chi} \tag{32}$$

$$(a+b)\mathbf{j}^+ + (a-b)\mathbf{j}^- = \boldsymbol{\Pi}\mathbf{q} - \mathbf{G}^+ \mathbf{j}^+ - \mathbf{G}^- \mathbf{j}^-, \tag{33}$$

where the $\mathbf{G}_{\gamma\gamma'}^\pm$ matrices are given by Eq. (34).

$$\mathbf{G}_{\gamma\gamma'}^\pm = 2\boldsymbol{\Pi}_\gamma \mathbf{M}_{\gamma'}^+ (\boldsymbol{\Lambda}^T \mathbf{K}_{\gamma'}^T \mathbf{E}_{\gamma'}^T)^{-1} \otimes \mathbf{D}_{\gamma'} \pm \boldsymbol{\Pi}_\gamma \mathbf{M}_{\gamma'}^- \mathbf{K}_{\gamma'} \boldsymbol{\Lambda} \otimes \mathbf{D}_{\gamma'} \tag{34}$$

Solving for $\mathbf{j}^+$, the familiar response matrix equation given by Eq. (34) results, where the new matrices are defined in Eqs. (36) and (37).

$$\mathbf{j}^+ = \mathbf{R}\,\mathbf{j}^- + \mathbf{B}\,\mathbf{s} \tag{35}$$

$$\mathbf{R} = \left[(a+b)\mathbf{I} + \mathbf{G}^+ \right]^{-1} \left[(b-a)\mathbf{I} - \mathbf{G}^- \right] \tag{36}$$

$$\mathbf{B} = \left[(a+b)\mathbf{I} + \mathbf{G}^+ \right]^{-1} \boldsymbol{\Pi} \mathbf{A}^{-1} \mathbf{J} \otimes \mathbf{I}_s \tag{37}$$

The following section gives a brief discussion of some numerical results obtained for two benchmarks using the above method.

3. Modified Watanabe-Maynard

As stated earlier, the above matrix relationships have been implemented in MATHCAD and tested for stability and accuracy. In all of these tests, the first-order spherical harmonics method conserved neutrons and performed well. The response matrix formulation has been implemented in MATHCAD first because the angular matrices are far more difficult to implement in the existing VARIANT coding than in MATHCAD. The outer iteration solver in MATHCAD, however, can only solve problems of limited size (~50 nodes and low order approximations). To overcome this limitation, a patch was made for the VARIANT code, called VARIANT-F, so that VARIANT would perform the outer iterations using the response matrices obtained in MATHCAD.

The spherical harmonics method developed in Section 2 requires a complete odd-order expansion of spherical harmonics within the nodal domain. Along the interface we are free to use even- or odd-order sets of angular trial functions that obey Rumyantsev interface conditions [5] or the LI conditions [4]. As for the free parameters *a* and *b*, no theoretical justification has yet been established which would indicate optimum values. As a result, four different values of the free parameters *a* and *b* were considered. Our numerical studies have indicated that only the bounded $\boldsymbol{\varphi}_\gamma$ conditions (a = 2.0, b = 0.0) combined with a Rumyantsev interface trial function set yields acceptable solutions. The LI trial function set was eliminated because it did not result in solutions with asymptotic convergence towards the reference solution.

Several fixed-source, two-dimensional benchmark problems were used to test the new formulation. A simplification of a Watanabe-Maynard benchmark [6-7], shown in Fig. 1, displayed the largest errors and is discussed here. This benchmark was primarily used to assess the accuracy of the void treatment for the first-order formulation. The original benchmark defined a larger source region (shaded region) and smaller source magnitude than that shown in Fig. 1. The benchmark dimensions were simplified for this work to reduce the computational burden in MATHCAD.

The average flux within each node was used to assess the accuracy of the method rather than relying upon a rigorous reconstruction of the flux. All four flux traverses shown on the right hand side of Fig. 1 were investigated, but only a subset is presented here. The reference solution was obtained using the collision probability code DRAGON [6]. For perspective, discrete ordinate solutions were obtained using TWODANT [8].

Figure 2 gives the void flux traverse solutions for VARIANT-F using odd-order Rumyantsev interface conditions. Also included is a TWODANT S_{12} solution for comparison purposes. In general, the low order P_N solutions are very inaccurate near the source region and in the void region. However, the VARIANT-F solutions do eventually take up the shape of the reference DRAGON solution as the angular order is refined, but the accuracy is not very good. The TWODANT solutions display a little different behavior than the VARIANT-F solution. Near the source, the TWODANT solutions are very accurate, but in the void region and along the vacuum boundary (not shown), the ray effects lead to non physical characteristics.

The void flux traverse solutions for VARIANT-F using even-order Rumyantsev interface conditions are given in Fig. 3. Similar to the odd P_N solutions, the low order approximations are rather inaccurate near the source and void region. As the angular order is refined, clearly the VARIANT-F solutions tend to match the reference DRAGON solution.

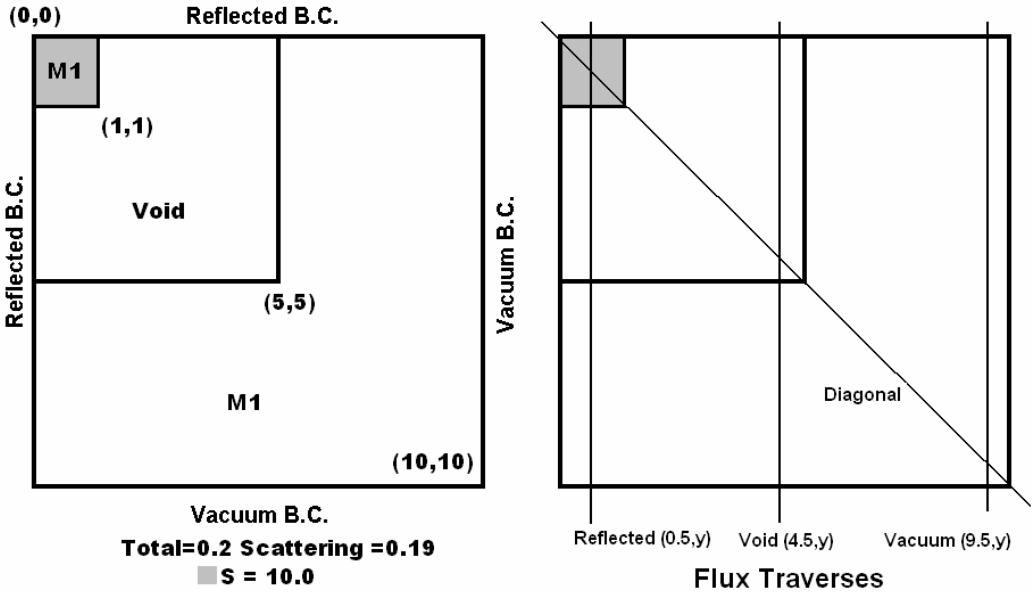

Fig. 1. Modified Watanabe-Maynard Benchmark Geometry

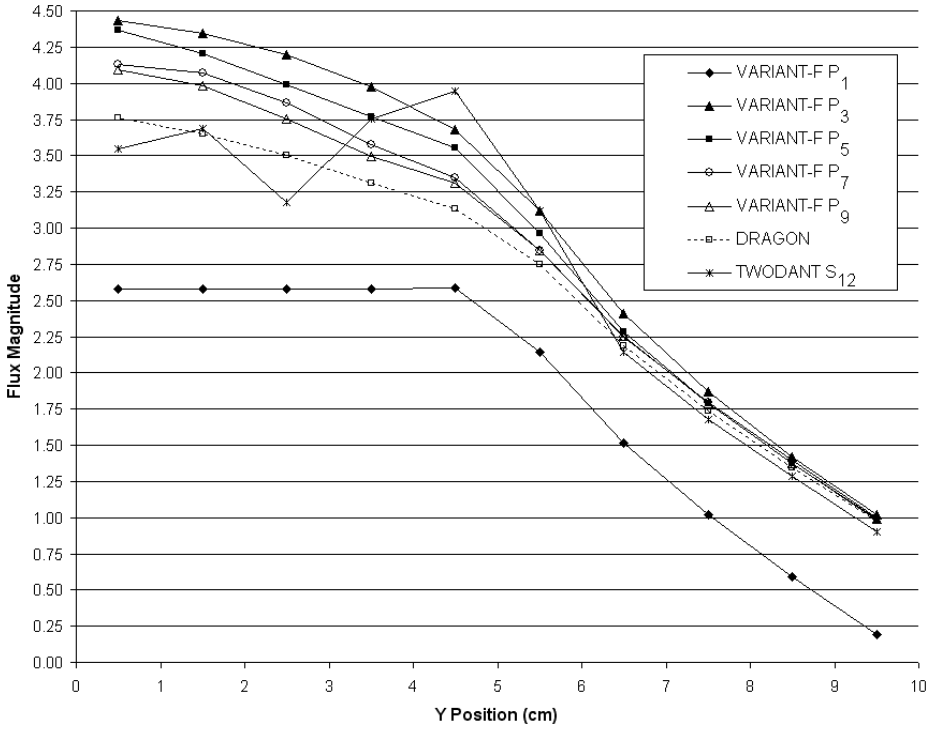

Fig. 2. Odd-order VARIANT-F Solutions to the Watanabe-Maynard Benchmark

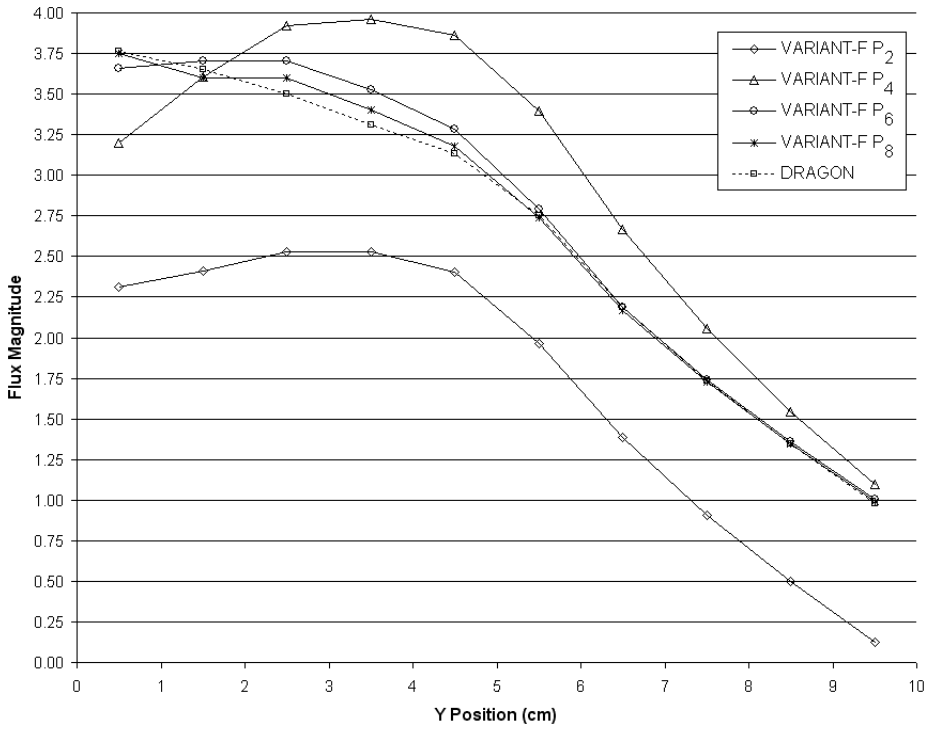

Fig. 3. Even-order VARIANT-F Solutions to the Watanabe-Maynard Benchmark

It is important to note that only some of the odd-order VARIANT-F solutions succeeded in reaching the desired convergence of 10^{-6} on the flux while in some cases the outer iteration procedure was stopped when the convergence error was less than 10^{-4}. The spectral radius of the lower order odd P_N problems was computed to be near 1.0 which makes the solution of the system of equations difficult at best. As the angular order is increased the spectral radius does improve and a converged solution (10^{-6}) was possible using P_9. Unlike the odd-order VARIANT-F solutions, there were no significant convergence problems with the even-order VARIANT-F solutions. Only a slight degradation in the spectral radius was observed as the angular order was increased.

At this point we can address the problem with the odd-order VARIANT-F solutions. In Section 2, we stated that an odd-order spherical harmonics approximation within the domain, or in Eq. (15), is necessary for the inversion in Eq. (16) regardless of the interface approximation. For the preceding odd-order VARIANT-F solutions we have assumed that the internal odd-order matched that of the order applied along the boundary. For the even-order VARIANT-F solutions the internal odd-order approximation clearly had to be greater than the even-order (P_2 on the boundary requires P_3 inside). The fundamental problem with the odd-order method is first seen in Eq. (17) or its discretized form, Eq. (22).

In Eq. (22), we are linking the incoming neutron flux entering the nodal domain to a set of spherical harmonic functions which are continuous across the nodal interface. The underlying subtlety is that the use of continuous angular trial functions actually defines both the incoming and outgoing angular distribution of neutrons along the boundary. For odd-order VARIANT-F solutions this amounts to over-constraining the angular dependence of the flux since the angular order within the domain is the same as that along the boundary. We can draw parallels to the spatial domain to further explain this. Assuming we used a 6^{th} order polynomial expansion of the flux (spatial) within the domain, we obviously cannot employ a 6^{th} order spatial approximation to the flux along the boundary since the resulting system of equations would be rank deficient.

The success of the even-order approximation comes from the fact that it bounds the magnitude of key higher order angular terms but does not explicitly bound all of the terms on each surface. Additional work has been initiated to determine the proper odd-order boundary conditions which would be compatible with the VARIANT code and not lead to the preceding accuracy and convergence problems. These conditions would obviously have odd-order interface conditions that are of lower order than that used internal to the node (P_1 along the boundary using P_3 inside, etc…). At this point the P_1 conditions have generally been found to be convergent using any higher order angular approximation within the nodal domain.

4. Conclusions

For the Watanabe-Maynard benchmark, the first-order form using odd-order interface conditions had substantial inaccuracies and displayed significant convergence problems attributed to an over-constrained angular flux. With even-order interface conditions, there was still significant error, but no convergence problems were present.

In general, the solutions obtained using VARIANT-F proved to have the correct flux shape, but an insufficient space-angle approximation and slow convergence in the outer iterations prevented it from obtaining accurate solutions. Overall the new method does appear to be able to treat void regions although a higher order angular approximation is clearly necessary for problems containing voids. From a researcher's viewpoint, it is quite gratifying to be able to

demonstrate a method capable of treating void regions that is based explicitly on the spherical harmonics method. To our knowledge, this is the first time this has been achieved. Most importantly, the new formulation is compatible with the existing second-order method available in the VARIANT code.

As a final note, additional research has shown that a nodal first-order integral method compatible with a recent second-order integral method [9] can also treat void problems. This integral method is computationally more efficient and generally more accurate (with respect to angular order) than the preceding first-order spherical harmonics method.

Acknowledgements

This work was supported by the U.S. Department of Energy under Contract numbers DE-FG07-01ID1410 and W-31-109-Eng-38.

References

1) C. B. Carrico, E.E. Lewis and G. Palmiotti, "Three Dimensional Variational Nodal Transport Methods for Cartesian, Triangular and Hexagonal Criticality Calculations," Nucl. Sci. Eng. 111, 168 (1992).
2) G. Palmiotti, E. E. Lewis & C. B. Carrico, "VARIANT: VARIational Anisotropic Nodal Transport for Multidimensional Cartesian and Hexagonal Geometry Calculation," Argonne National Laboratory ANL-95/40, 1995.
3) Mathsoft, Mathcad 6.0 Professional Edition Users Manual. Mathsoft, 1995.
4) G. Palmiotti, C. B. Carrico, and E. E. Lewis, "Variational Nodal Transport Methods with Anisotropic Scattering," Nucl. Sci. Eng. 115, 233-234 (1993).
5) W. S. Yang, M. A. Smith, G. Palmiotti & E. E. Lewis, "Interface Conditions and Angular Trial Functions in Variational Nodal Formulation for Multi-dimensional Spherical Harmonics Method," to be submitted to Nucl. Sci. Eng. (2003).
6) G. Marleau, A. Hébert & R. Roy, "A User's Guide for DRAGON," Ecole Polytechnique de Montréal, December 1997.
7) Y. Watanabe and C. W. Maynard, "The discrete cones method in two dimensional neutron transport computations," University of Wisconsin. Report UWFDM-574 (1984).
8) R. E. Alcouffe, F. W. Brinkley, D. R. Marr, and R. D. O'dell, "User's Guide for TWODANT: A Code Package for Two-Dimensional, Diffusion-Accelerated Neutral Particle Transport," LA-10049-M, Los Alamos National Laboratory (1984).
9) M. A. Smith, G. Palmiotti, E. E. Lewis & N. Tsoulfanidis, "An Integral Form of the Variational Nodal Method," to be published in Nucl. Sci. Eng. (2004).